Journal of Zhejiang University-SCIENCE B 2025 26(12):1260-1268
www.jzus.zju.edu.cn; www.springer.com/journal/11585
E-mail: jzus_b@zju.edu.cn

Correspondence

https://doi.org/10.1631/jzus.B2400163

Check for updates

Drug-assisted synthesis of copper nanoparticles and their induction of cuproptosis and necrosis for breast cancer therapy

Yuewen WANG[1], Jingjie GAO[1], Yuying CHENG[1], Hanling PAN[1], Hanxiao TANG[2], Chenguang LIU[1]✉

[1]*Zhejiang Provincial Engineering Research Center of New Technologies and Applications for Targeted Therapy of Major Diseases, College of Life Sciences and Medicine, Zhejiang Sci-Tech University, Hangzhou 310018, China*
[2]*Academy of Chinese Medical Sciences, Henan University of Chinese Medicine, Zhengzhou 450046, China*

Neurokinin-1 receptor (NK1R), a member of the G protein-coupled receptor (GPCR) family, contributes to multiple pathological processes, including pain, chronic inflammation, and cancer (Gutierrez et al., 2019; Robinson et al., 2023). Current reports and our previous work have proven that NK1R is highly expressed in many cancer cells, such as colorectal cancer and leukemia, and that targeted blocking of NK1R can effectively inhibit tumor cell proliferation (Li XQ et al., 2013; Li JY et al., 2016; Ge et al., 2019; Shi et al., 2021). In addition, GPCRs have been found not only in the plasma membrane but also in the membranes of endosomes and lysosomes with endocytosis (Irannejad et al., 2017; Yarwood et al., 2017), which is more pronounced in cancer cells with highly developed lysosomes (Ramírez-García et al., 2019).

Aprepitant, an NK1R antagonist approved by the United States Food and Drug Administration (FDA), can effectively block the overexpression of NK1R in cancer cells (Yuan et al., 2016). Nevertheless, its poor aqueous solubility and low bioavailability greatly limit its application in cancer therapy (Shadle et al., 2012). In recent years, drug–metal coordination nanoparticles have attracted extensive research interest because such nanoparticles consist of single or multiple small molecules (e.g., curcumin and indocyanine green) and metal ions, thus constructing carrier-free nanoparticles that reach the nanoscale while dramatically increasing the proportion of active component (Lin et al., 2021; Zhou et al., 2022).

Copper (Cu), as a transition metal, has been extensively utilized in the fabrication of self-assembled nanoparticles due to its excellent coordination capabilities (Zhu et al., 2024a). Unlike conventional systems that depend on drug adsorption or encapsulation within organic or inorganic nanomaterials (Guan et al., 2023; Wong et al., 2024), drug–metal coordination nanoparticles leverage the direct coordination between metal ions and drug molecules. This unique property classifies them as carrier-free nanodrugs, which offer significantly higher drug-loading efficiency than traditional delivery systems. Beyond serving as a structural component for nanodrug formulations, copper also exhibits intrinsic therapeutic potential. Copper has emerged as a key mediator of novel cell-death pathways, including cuproptosis and ferroptosis, which are characterized by regulated cell-death mechanisms that are dependent on metabolic and oxidative stress (Liu et al., 2023; Li et al., 2024; Zhu et al., 2024b). Cuproptosis has a shorter development period, and Tsvetkov et al. (2022) revealed its mechanism, in which cell death is induced by targeting lipoylated tricarboxylic acid (TCA) cycle proteins. Excessive copper(I) (Cu^+) ions bind to lipoylated dihydrolipoamide *S*-acetyltransferase (DLAT), further leading to DLAT oligomerization (Yang LF et al., 2023). Cu^+-induced decrease in Fe-S stabilization or inactivation of Npl4-p97 also results in copper-induced cell death (Xie et al., 2023). Building on these findings, copper ion-based nanomaterials, such as copper sulfide nanoparticles and copper-based metal-organic-framework nanoparticles, have demonstrated potent

✉ Chenguang LIU, cgliu@zstu.edu.cn
Chenguang LIU, https://orcid.org/0000-0001-5999-8870

Received Mar. 25, 2024; Revision accepted Dec. 26, 2024; Crosschecked Dec. 18, 2025

anti-tumor effects by inducing cellular cuproptosis (Liu et al., 2022; Tong et al., 2023; Hu et al., 2024). For instance, Zhu et al. (2024a) successfully developed carrier-free nano-sonosensitizers through self-assembly of copper(II) (Cu^{2+}) and chlorin e6, enabling efficient Cu^{2+} delivery and inducing multiple cell-death pathways, including cuproptosis. However, to the best of our knowledge, there has been limited research on the application of Cu^{0}-based nanomaterials in cuproptotic cancer therapy. This is largely due to their high susceptibility to oxidation when exposed to aqueous environments, which poses significant challenges for maintaining their stability and functionality (Chung et al., 2022).

Considering that both cuproptosis and NK1R blockade-induced cell death are closely associated with mitochondria, we employed the NK1R antagonist aprepitant here to assist in the preparation of copper nanoparticles (Cu-aprepitant NPs) and to improve their antioxidant properties. The construction of Cu-aprepitant NPs greatly improved the water solubility of aprepitant. The obtained Cu-aprepitant NPs exhibited a favorable low-pH response for drug release and physiological-environmental stabilization. As copper in Cu-aprepitant NPs was oxidized to copper ions, particularly in tumor cells with high metabolic and reactive oxygen species (ROS) levels, they effectively induced cuproptosis in breast cancer cells. Meanwhile, the released aprepitant also blocked the highly expressed NK1R in breast cancer cells, thereby inducing synergistic cell death (Fig. 1). Thus, these rapidly synthesized carrier-free Cu-aprepitant NPs were able to kill breast cancer cells efficiently, and our findings can be generalized to other drug-assisted preparations of metal nanoparticles and cancer multi-pathway therapies.

In this study, we synthesized copper nanoparticles by introducing an FDA-approved NK1R antagonist, aprepitant, which has been reported to have a good anti-cancer effect (Ge et al., 2019). The preparation and characterization methods for Cu-aprepitant NPs are provided in the supplementary Materials

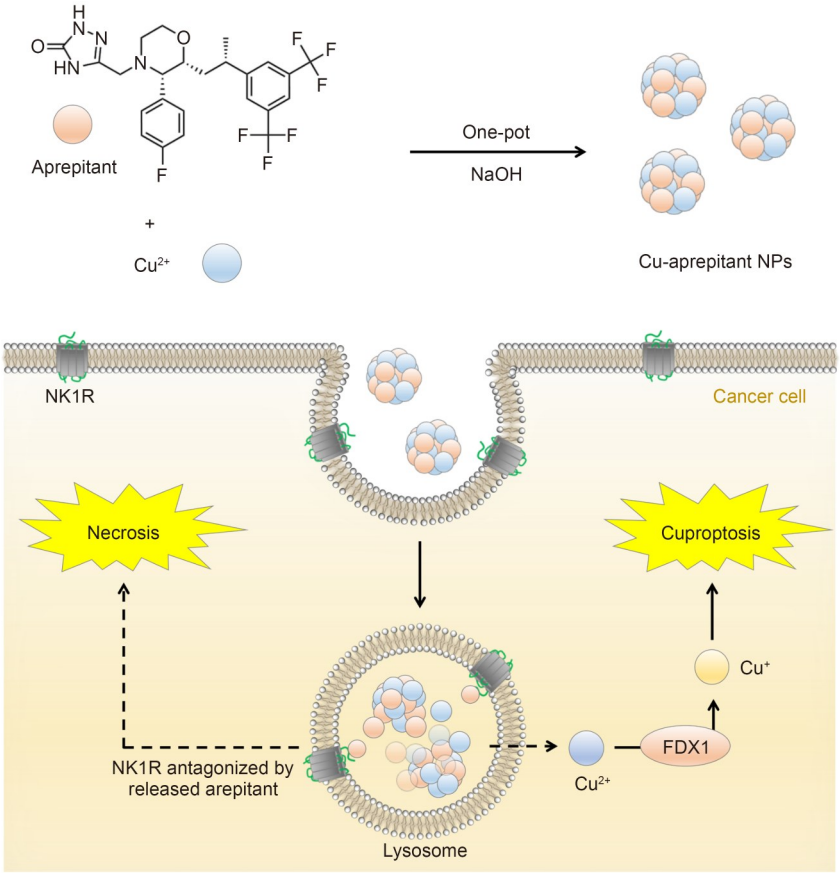

Fig. 1 Illustration of the one-pot method for synthesizing Cu-aprepitant nanoparticles (NPs) and the cell-death pathways assisted by Cu-aprepitant NPs.

and Methods section. Fig. 2a shows the absorption spectra of the aprepitant solution, $CuCl_2$ solution, mixture of $CuCl_2$ and aprepitant, mixed systems at the beginning of the reaction (i.e., Cu-aprepitant seeds), and Cu-aprepitant NPs. The ultraviolet-visible (UV-Vis) absorption spectra of Cu-aprepitant seeds and Cu-aprepitant NPs revealed distinct changes during the formation process. A broad increase in absorption was observed in the range of 300–450 nm, accompanied by a significant decrease in the characteristic absorption peak at approximately 290 nm, which is typically attributed to free Cu^{2+} ions. Additionally, the ligand-to-metal charge transfer (LMCT) transitions, commonly found in the 200–400 nm region, exhibited enhanced absorption (Su et al., 2023), further indicating structural and electronic changes associated with coordination between copper ions and aprepitant. These results demonstrate that during the synthesis process of Cu-aprepitant NPs, the copper nanoparticles continued to grow and the Cu-aprepitant complexes formed via coordination between the nitrogen (N) atoms of aprepitant and copper in the presence of OH^- ions. Scanning electron microscopy (SEM) (Fig. 2b) and transmission electron microscopy (TEM) (Fig. 2c) images display the morphology of Cu-aprepitant NPs. The Cu-aprepitant NPs resulted in spherical particles with a size of (50.56±11.77) nm (n=200), a polydispersity index (PDI) of 0.25±0.02, and a zeta potential of (34.7±0.7) mV, indicating good homogeneity and water stability of the obtained Cu-aprepitant NPs.

Energy-dispersive spectrometry (EDS) revealed the existence of Cu and elements, including N and F, contained in the aprepitant in the as-obtained Cu-aprepitant NPs (Fig. 2d). To confirm the percentage of each component in Cu-aprepitant NPs, we collected the resultant Cu-aprepitant NPs by centrifugation and measured the unloaded aprepitant in the supernatant by high-performance liquid chromatography (HPLC). The drug-loading content (DLC) was (78.2±4.4)%. Meanwhile, the freeze-dried Cu-aprepitant NPs were ablated with aqua regia, and then the concentration of copper was determined using the inductively coupled plasma-optical emission spectroscopy (ICP-OES). The results showed that the mass percentage of copper in Cu-aprepitant NPs was 18.91%, i.e., the molar ratio of copper atoms to aprepitant (molecular weight=534.43 Da) in Cu-aprepitant NPs was approximately 2:1.

To explore the possible interactions between copper ions and aprepitant, we recorded the Fourier-transform infrared (FTIR) spectra of Cu-aprepitant NPs.

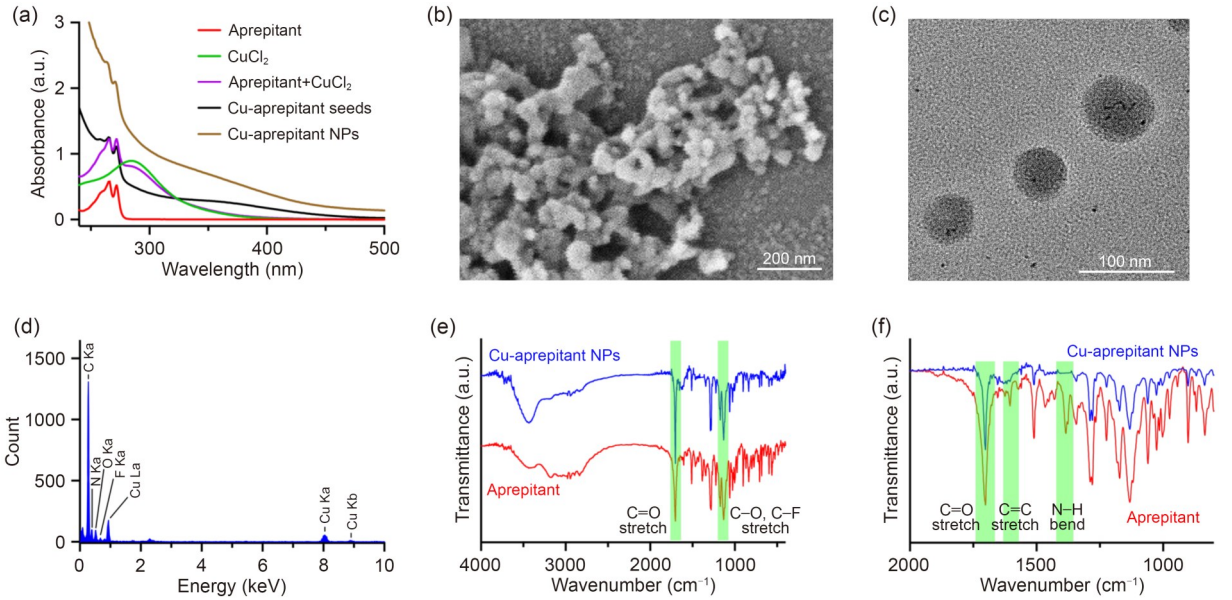

Fig. 2 Characterization of Cu-aprepitant nanoparticles (NPs). (a) Ultraviolet-visible (UV-Vis) spectra of aprepitant, $CuCl_2$, mixture of aprepitant and $CuCl_2$, Cu-aprepitant seeds, and Cu-aprepitant NPs. (b, c) Scanning electron microscopy (SEM) (b) and transmission electron microscopy (TEM) (c) images of Cu-aprepitant NPs. (d) Energy-dispersive spectrometry (EDS) of Cu-aprepitant NPs. (e) Full-range Fourier-transform infrared (FTIR) spectra of Cu-aprepitant NPs and aprepitant. (f) Zoomed-in regions of the FTIR spectra showing differences in the N–H bending for Cu-aprepitant NPs and aprepitant. a.u.: arbitrary unit.

As shown in Figs. 2e and 2f, the characteristic bands of aprepitant at 1703 and 1608 cm^{-1} could be attributed to the stretching vibrations of single-bond C=O and C=C, respectively (Yeo et al., 2020; Nogusa et al., 2023). The bending vibration of N–H at 1452 cm^{-1} disappeared due to the coordination of nitrogen and copper (Fig. 2f). These results indicate that the construction of Cu-aprepitant NPs does not change the overall structure of the aprepitant, and the copper ions in the nanoparticles are bound together by coordination with the nitrogen atoms in the aprepitant.

In addition, we used the X-ray diffraction (XRD) spectra to compare the structural identities of aprepitant and Cu-aprepitant NPs. As shown in Fig. 3a, the peaks of aprepitant are indexed to the pattern of Cu-aprepitant NPs but with lower intensities, which we attribute to a higher proportion of copper in the Cu-aprepitant NPs (Pan et al., 2020). The peaks at diffraction angles (2θ) of 43.94°, 51.13°, and 75.37° can also be observed in the pattern, and correspond to the characteristic face-centered cubic (FCC) symmetry of the copper lines indexed at (111), (200), and (222), respectively (Upadhyay and Kumar, 2017; Wang et al., 2020). In comparison, the mixed powder of reaction substrates (i.e., $CuCl_2$ and aprepitant) exhibited weak peaks for aprepitant and $CuCl_2$ (Jianu et al., 2016). The composition details were also reflected by X-ray photoelectron spectroscopy (XPS) characterization techniques, which showed that Cu-aprepitant NPs were composed of C, N, O, F, and Cu elements (Fig. 3b), which was consistent with the EDS results. In the Cu 2p XPS spectra (Fig. 3c), the peaks indicating the metallic copper state were substantially larger for Cu-aprepitant NPs (Kim et al., 2021). No strong Cu^{2+} satellite peaks were visible in the Cu 2p XPS spectra of Cu-aprepitant NPs, while the broad satellite peak (943.9 eV) was observed in the mixture of $CuCl_2$ and aprepitant, indicating that there was Cu^{2+} in the mixture and a decrease in this component in Cu-aprepitant NPs (Platzman et al., 2008; Wang et al., 2020). A slight peak displacement can be seen in the N 1s spectra (Fig. 3d). This is because in the growth process of Cu-aprepitant NPs, there were a few Cu^{+} states in Cu-aprepitant NPs and they were coordinated with the nitrogen in the aprepitant (Sun et al., 2022).

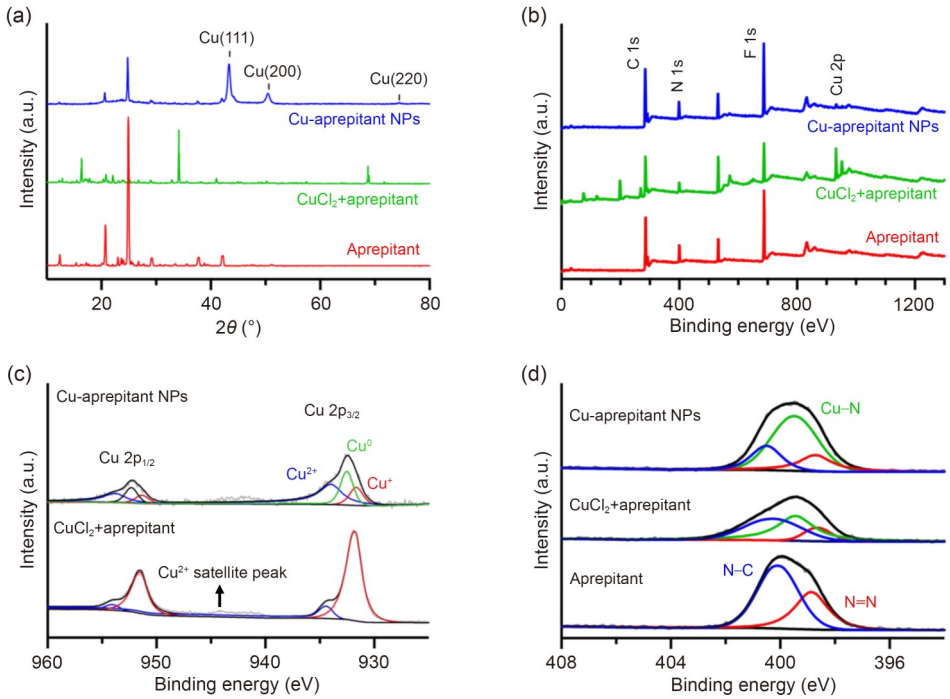

Fig. 3 Phase and chemical-state investigation of Cu-aprepitant nanoparticles (NPs). (a) X-ray diffraction (XRD) spectra of Cu-aprepitant NPs, mixture of $CuCl_2$ and aprepitant, and aprepitant powder. (b) Overall X-ray photoelectron spectroscopy (XPS) spectra of Cu-aprepitant NPs, mixture of $CuCl_2$ and aprepitant, and aprepitant powder. (c) Cu 2p peak of Cu-aprepitant NPs and the mixture of $CuCl_2$ and aprepitant. (d) N 1s peak of Cu-aprepitant NPs, mixture of $CuCl_2$ and aprepitant, and aprepitant powder. a.u.: arbitrary unit.

Due to the reduced coordination interaction between copper and aprepitant under acidic conditions, Cu-aprepitant NPs have the potential to dissolve in lysosomes and release Cu^{2+} and aprepitant. To investigate aprepitant release, we treated Cu-aprepitant NPs in a variety of simulated in vivo pH environments (pH 7.4 for the normal environment, pH 6.8 for the tumor microenvironment, and pH 5.7 for the endosomes or lysosomes). Fig. 4a shows the cumulative release of aprepitant from Cu-aprepitant NPs. In physiological (pH 7.4) and weak acid (pH 6.8) buffers, the aprepitant slightly increased during the first 12 h and then remained stable. In comparison, the Cu-aprepitant NPs in buffer at pH 5.7 exhibited more rapid drug release, with a 24-h drug-release rate of approximately 78%. The pH-responsive release of aprepitant is due mainly to acidic conditions with high H^+ concentrations, in which protons compete with the electron donor (nitrogen) in aprepitant, thus weakening its bond to copper ions (Zheng et al., 2011, 2013). Moreover, as the surface copper ions dissociate from aprepitant, the exposed monomeric copper continues to be oxidized, accelerating the degradation of Cu-aprepitant NPs and aprepitant release.

We were able to determine the long-term stability of Cu-aprepitant NPs in physiological environments. The UV-Vis spectra of Cu-aprepitant NPs after 16 d of storage were not significantly different from those of the freshly made samples (Fig. 4b). In addition, the size of Cu-aprepitant NPs after two weeks of storage in the cell culture medium was slightly increased but within a reasonable range, which can be attributed to protein adhesion. Meanwhile, the hydrated particle size and PDI of Cu-aprepitant NPs after four weeks of storage significantly increased (Fig. 4c), and the zeta potential became (−7.2±0.2) eV, indicating the disintegration and reaggregation of nanoparticles. These results indicate that Cu-aprepitant NPs have a stable structure and composition within two weeks in the physiological environment.

Before determining the anti-cancer effects of Cu-aprepitant NPs, we observed the cellular uptake of fluorescein isothiocyanate (FITC)-labeled Cu-aprepitant NPs with confocal laser scanning microscopy (CLSM). As shown in Fig. 4d, the green fluorescence attributed to FITC-labeled Cu-aprepitant NPs was localized within the cells and mostly overlapped with the red fluorescence attributed to lysosomes, resulting in yellow or orange colors in the merged image. This suggested that Cu-aprepitant NPs entered the human breast cancer cell line (SKBR3) cells by endocytosis after 3 h of co-incubation. In an acidic environment (Fig. 4a), Cu-aprepitant NPs, which are sensitive to acidic conditions, can quickly release the aprepitant

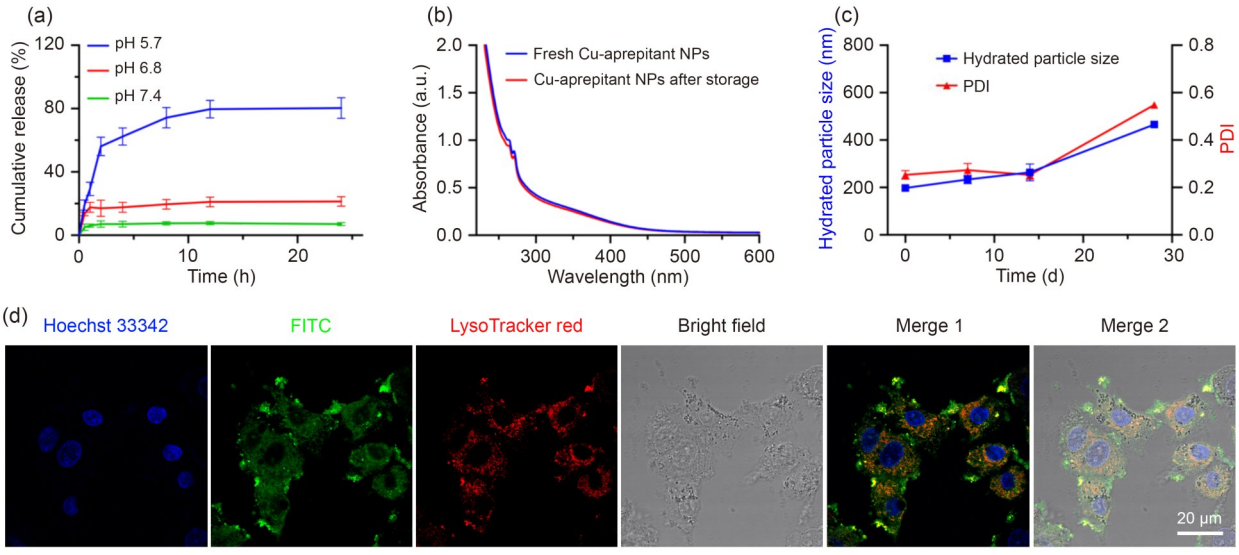

Fig. 4 In vitro drug release, water-stability, and cellular internalization of Cu-aprepitant nanoparticles (NPs). (a) Cumulative release of aprepitant from Cu-aprepitant NPs. (b) Ultraviolet-visible (UV-Vis) spectra of freshly prepared Cu-aprepitant NPs and Cu-aprepitant NPs after 16 d of storage. (c) Hydrated particle size and polydispersity index (PDI) of Cu-aprepitant NPs after storage in the physiological environment. (d) Cellular uptake of Cu-aprepitant NPs after 3 h of co-incubation with the human breast cancer cell line (SKBR3) cells. (a, c) The data were expressed as mean±standard deviation (SD), *n*=3. a.u.: arbitrary unit; FITC: fluorescein isothiocyanate.

and copper nanoparticles in the lysosome to exert a cytostatic effect by blocking NK1R on the lysosomal membrane and inducing cuproptosis (Ramírez-García et al., 2019).

To evaluate the cytotoxicity of Cu-aprepitant NPs compared to free aprepitant in normal cells, both formulations were co-incubated with human umbilical-vein endothelial cells (HUVECs) for 24 h. As shown in Fig. 5a, HUVECs treated with free aprepitant exhibited concentration-dependent cytotoxicity, with a half maximal inhibitory concentration (IC_{50}) of 0.018 mmol/L. In contrast, HUVECs exposed to Cu-aprepitant NPs under the same conditions showed negligible cytotoxicity. Subsequently, we selected two human breast cancer cell lines, SKBR3 and MDA-MB-231, as models to investigate the in vitro anti-cancer effects of Cu-aprepitant NPs. After 24 h of treatment with graded concentrations of Cu-aprepitant NPs, both SKBR3 and MDA-MB-231 cells exhibited concentration-dependent inhibition of proliferation. Specifically, SKBR3 cell viability decreased to (21.34±3.37)% at a Cu-aprepitant NP concentration of 100 μg/mL (i.e., 0.30 mmol/L aprepitant; Fig. 5b), while MDA-MB-231 cells also showed a significant reduction in viability (Fig. S1). The IC_{50} values of Cu-aprepitant NPs were calculated to be 27.93 μg/mL for SKBR3 cells and 92.83 μg/mL for MDA-MB-231 cells, demonstrating a higher sensitization of SKBR3 to Cu-aprepitant NPs. The difference in toxicity of free aprepitant and Cu-aprepitant NPs between HUVECs and breast cancer cells primarily arises from the distinct localization of NK1R. In normal cells, NK1R is predominantly located on the extracellular membrane, where it readily binds to and is inhibited by aprepitant. In contrast, in tumor cells, NK1R is translocated to lysosomes (Ramírez-García et al., 2019). As a result, Cu-aprepitant NPs internalized via endocytosis accumulate in lysosomes, leading to enhanced cytotoxicity in SKBR3 or MDA-MB-231 cells. As previously reported, the cytotoxicity of the free drug in two-dimensional (2D) cell-culture models might be comparable to, or even greater than, that of nanoparticles at equivalent drug concentrations (Némati et al., 1994; Norouzi et al., 2020). This is due to the rapid

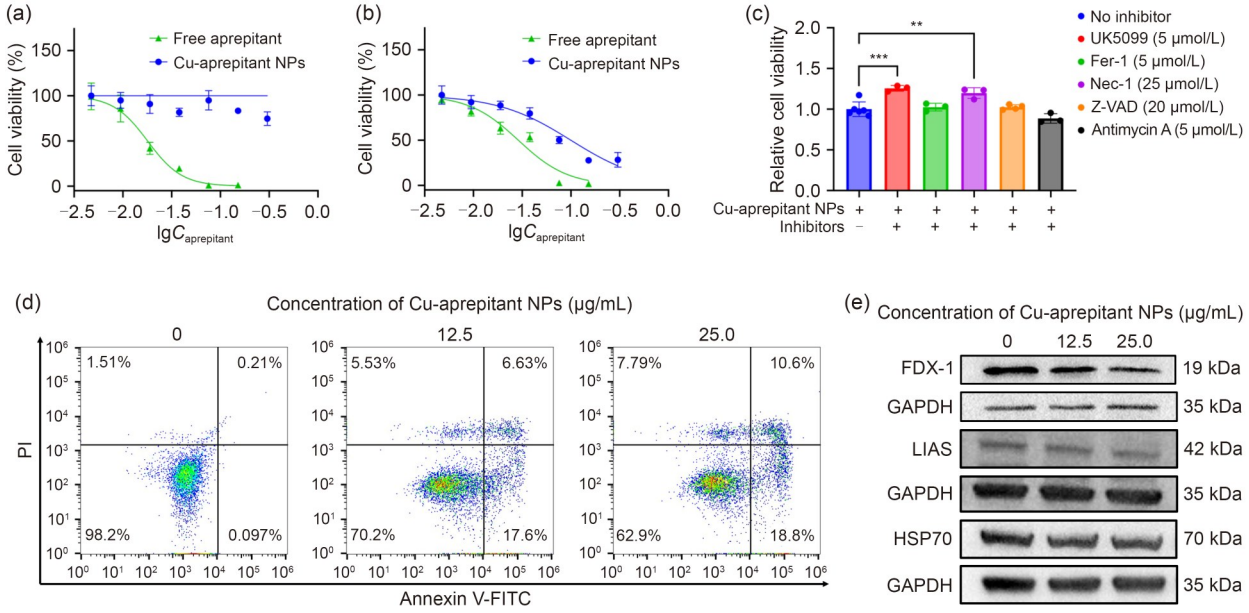

Fig. 5 In vitro anti-cancer effect and pathways of Cu-aprepitant nanoparticles (NPs). (a, b) Viability of human umbilical-vein endothelial cells (HUVECs) (a) and SKBR3 cells (b) cultured with gradient concentrations of free aprepitant and Cu-aprepitant NPs. (c) Relative viability of SKBR3 cells after co-incubation with inhibitors and Cu-aprepitant NPs (25.0 μg/mL). (d) Flow cytometry of cell apoptosis rates (%) of SKBR3 cells after co-incubation with Cu-aprepitant NPs (12.5 and 25.0 μg/mL). (e) Western blot analysis of SKBR3 cells treated with Cu-aprepitant NPs for 24 h. The data are expressed as mean±standard deviation (SD), n=3. $^{**}P$<0.01; $^{***}P$<0.001. PI: propidium iodide; FITC: fluorescein isothiocyanate; $C_{aprepitant}$: concentration of aprepitant (mmol/L); UK5099: α-cyano-β-(1-phenylindol-3-yl)acrylate; Fer-1: ferrostatin-1; Nec-1: necrostatin-1; Z-VAD: Z-Val-Ala-Asp(OMe)-fluoromethylketone; FDX-1: ferredoxin-1; LIAS: lipoyl synthase; HSP70: heat shock protein 70; GAPDH: glyceraldehyde-3-phosphate dehydrogenase.

penetration and direct diffusion of the free drug into the cells, creating high local concentrations that enhance its cytotoxic effects.

To further verify the pathway by which Cu-aprepitant NPs induced cell death, SKBR3 cells were pre-treated with high, medium, or low concentrations of inhibitors of cuproptosis, ferroptosis, necrosis, apoptosis, and the mitochondrial respiratory chain (i.e., α-cyano-β-(1-phenylindol-3-yl)acrylate (UK5099), ferrostatin-1 (Fer-1), necrostatin-1 (Nec-1), Z-Val-Ala-Asp(OMe)-fluoromethylketone (Z-VAD), and antimycin A), and then co-cultured with Cu-aprepitant NPs. The results showed that cuproptosis and necrosis inhibitors could reverse cell cytostasis, while the others had no reversal effect (Fig. 5c). Previous studies by our team have verified that aprepitant blocks NK1R and activates endoplasmic reticulum stress, programming the necrosis of cells (Ge et al., 2019; Shi et al., 2021). The released aprepitant from Cu-aprepitant NPs consistently contributed to cell necrosis. The reversal of cell death by cuproptosis inhibitor UK5099 confirmed that copper components in Cu-aprepitant NPs underwent a valence shift upon cellular uptake and induced cuproptosis. Fig. 5d depicts the apoptosis rates as measured by flow cytometry. Treatments with Cu-aprepitant NPs at concentrations of 12.5 and 25.0 μg/mL induced apoptotic cell populations of 24.23% and 29.40%, respectively, significantly higher than that in the negative control group (0.31%). This increase is likely attributable to the apoptosis-like features of cuproptotic cells and the necrotic effects induced by aprepitant (Ge et al., 2019; Pi et al., 2023). Notably, the incomplete apoptotic characteristics of cuproptotic cells, as detected by Annexin V/propidium iodide (PI)-based flow cytometry (Yang WC et al., 2023; Zhang et al., 2023), resulted in lower observed apoptotic populations compared to the total cell death measured using the cell counting kit-8 (CCK-8) assay. Western blot analysis further confirmed the occurrence of cuproptosis, as evidenced by the reduced expression of ferredoxin-1 (FDX-1) in SKBR3 cells after treatment with Cu-aprepitant NPs (Figs. 5e and S2). Additionally, the expression of lipoyl synthase (LIAS), which encodes components or protein targets involved in lipoylation (including DLAT), decreased in a concentration-dependent manner following Cu-aprepitant NP treatment. This suggests that Cu-aprepitant NPs promote DLAT lipoylation and subsequent oligomerization, thereby inducing cellular cuproptosis. Interestingly, no significant change was observed in the expression of heat shock protein 70 (HSP70), a protein typically upregulated during cuproptosis due to proteotoxic stress. This discrepancy could be explained by the release of HSP70 into the extracellular matrix, lysosomal rupture, or activation of proteases such as caspases and calpains, which can lead to HSP70 degradation (Gyrd-Hansen et al., 2004; Korbelik et al., 2005). These degradation processes, commonly associated with necrosis, suggest a necrotic component in the observed cell death (Brojatsch et al., 2014).

In conclusion, we successfully prepared copper nanoparticles with the FDA-approved NK1R antagonist aprepitant as a ligand and verified, for the first time, Cu^0-based nanoparticles capable of inducing cuproptosis. This drug-assisted synthesis of copper nanoparticles preserved the functionality of the drug. The aprepitant in this study exhibited a faster release rate in the simulated acidic environment of the lysosome and acted on the NK1R on the lysosomal membrane after endocytosis, thereby inducing necrosis. Combining the functions of copper and aprepitant, Cu-aprepitant NPs exhibited an effective in vitro inhibition of breast cancer cells by inducing cellular cuproptosis and necrosis. We hope that our study will be an impetus for the synthesis of drug-assisted copper nanoparticles and the design of nanoplatforms that synergize cuproptosis and other anti-cancer pathways by selecting different drugs.

Data availability statement

All the data generated or analyzed during this study are included in this published article and its supplementary information files.

Acknowledgments

This work was supported by the National Natural Science Foundation of China (No. 32201092) and the Zhejiang Provincial Natural Science Foundation of China (No. LTGY24H180008).

Author contributions

Yuewen WANG and Jingjie GAO performed the investigation and data curation. Yuying CHENG performed the methodology and data curation. Hanling PAN contributed to the investigation and writing – original draft. Hanxiao TANG was in charge of methodology and supervision. Chenguang LIU contributed to supervision, writing – review & editing, and funding acquisition. All authors have read and approved the

final manuscript, and therefore, have full access to all the data in the study and take responsibility for the integrity and security of the data.

Compliance with ethics guidelines

Yuewen WANG, Jingjie GAO, Yuying CHENG, Hanling PAN, Hanxiao TANG, and Chenguang LIU declare that they have no conflicts of interest.

All institutional and national guidelines for the care and use of laboratory animals were followed. This study was approved by the Research Ethics Committee of Zhejiang Sci-Tech University (No. 20220308-01).

References

Brojatsch J, Lima H, Kar AK, et al., 2014. A proteolytic cascade controls lysosome rupture and necrotic cell death mediated by lysosome-destabilizing adjuvants. *PLoS ONE*, 9(6):e95032. https://doi.org/10.1371/journal.pone.0095032

Chung K, Bang J, Thacharon A, et al., 2022. Non-oxidized bare copper nanoparticles with surface excess electrons in air. *Nat Nanotechnol*, 17(3):285-291. https://doi.org/10.1038/s41565-021-01070-4

Ge CT, Huang HM, Huang FY, et al., 2019. Neurokinin-1 receptor is an effective target for treating leukemia by inducing oxidative stress through mitochondrial calcium overload. *Proc Natl Acad Sci USA*, 116(39):19635-19645. https://doi.org/10.1073/pnas.1908998116

Guan HQ, Harris C, Sun SH, 2023. Metal–ligand interactions and their roles in controlling nanoparticle formation and functions. *Acc Chem Res*, 56(12):1591-1601. https://doi.org/10.1021/acs.accounts.3c00156

Gutierrez S, Alvarado-Vázquez PA, Eisenach JC, et al., 2019. Tachykinins modulate nociceptive responsiveness and sensitization: in vivo electrical characterization of primary sensory neurons in tachykinin knockout (Tac1 KO) mice. *Mol Pain*, 15:1744806919845750. https://doi.org/10.1177/1744806919845750

Gyrd-Hansen M, Nylandsted J, Jäättelä M, 2004. Heat shock protein 70 promotes cancer cell viability by safeguarding lysosomal integrity. *Cell Cycle*, 3(12):1484-1485. https://doi.org/10.4161/cc.3.12.1287

Hu HL, Zhang WW, Lei L, et al., 2024. Combination losartan with hyaluronic acid modified diethyldithiocarbamate loaded hollow copper sulfide nanoparticles for the treatment of breast cancer and metastasis. *Chin Chem Lett*, 35(3):108765. https://doi.org/10.1016/j.cclet.2023.108765

Irannejad R, Pessino V, Mika D, et al., 2017. Functional selectivity of GPCR-directed drug action through location bias. *Nat Chem Biol*, 13(7):799-806. https://doi.org/10.1038/nchembio.2389

Jianu OA, Lescisin M, Wang Z, et al., 2016. X-ray diffraction of crystallization of copper (II) chloride for improved energy utilization in hydrogen production. *Int J Hydrogen Energy*, 41(19):7848-7853. https://doi.org/10.1016/j.ijhydene.2015.12.213

Kim JY, Hong D, Lee JC, et al., 2021. Quasi-graphitic carbon shell-induced Cu confinement promotes electrocatalytic CO_2 reduction toward C_{2+} products. *Nat Commun*, 12:3765. https://doi.org/10.1038/s41467-021-24105-9

Korbelik M, Sun JH, Cecic I, 2005. Photodynamic therapy–induced cell surface expression and release of heat shock proteins: relevance for tumor response. *Cancer Res*, 65(3):1018-1026. https://doi.org/10.1158/0008-5472.1018.65.3

Li DY, Ha EN, Zhou ZL, et al., 2024. "Spark" PtMnIr nanozymes for electrodynamic-boosted multienzymatic tumor immunotherapy. *Adv Mater*, 36(13):2308747. https://doi.org/10.1002/adma.202308747

Li JY, Zeng Q, Zhang YX, et al., 2016. Neurokinin-1 receptor mediated breast cancer cell migration by increased expression of MMP-2 and MMP-14. *Eur J Cell Biol*, 95(10):368-377. https://doi.org/10.1016/j.ejcb.2016.07.005

Li XQ, Ma GD, Ma QY, et al., 2013. Neurotransmitter substance P mediates pancreatic cancer perineural invasion via NK-1R in cancer cells. *Mol Cancer Res*, 11(3):294-302. https://doi.org/10.1158/1541-7786.MCR-12-0609

Lin HR, Zhou Y, Wang JM, et al., 2021. Repurposing ICG enables MR/PA imaging signal amplification and iron depletion for iron-overload disorders. *Sci Adv*, 7(51):eabl5862. https://doi.org/10.1126/sciadv.abl5862

Liu CG, Fu CP, Shi YH, et al., 2022. Dual-responsive nanomotors for deep tumor penetration and subcellular arrangement. *Mater Des*, 222:111039. https://doi.org/10.1016/j.matdes.2022.111039

Liu CG, Guo LX, Wang Y, et al., 2023. Delivering metal ions by nanomaterials: turning metal ions into drug-like cancer theranostic agents. *Coord Chem Rev*, 494:215332. https://doi.org/10.1016/j.ccr.2023.215332

Némati F, Dubernet C, de Verdière AC, et al., 1994. Some parameters influencing cytotoxicity of free doxorubicin and doxorubicin-loaded nanoparticles in sensitive and multidrug resistant leucemic murine cells: incubation time, number of nanoparticles per cell. *Int J Pharm*, 102(1-3):55-62. https://doi.org/10.1016/0378-5173(94)90039-6

Nogusa T, Cooper CB, Yu ZA, et al., 2023. Tunable, reusable, and recyclable perfluoropolyether periodic dynamic polymers with high underwater adhesion strength. *Matter*, 6(7):2439-2453. https://doi.org/10.1016/j.matt.2023.04.007

Norouzi M, Yathindranath V, Thliveris JA, et al., 2020. Doxorubicin-loaded iron oxide nanoparticles for glioblastoma therapy: a combinational approach for enhanced delivery of nanoparticles. *Sci Rep*, 10:11292. https://doi.org/10.1038/s41598-020-68017-y

Pan YJ, Xu PY, Chen BQ, et al., 2020. Supercritical antisolvent process-assisted fabrication of chrysin-polyvinylpyrrolidone sub-microparticles for improved anticancer efficiency. *J Supercrit Fluids*, 162:104847. https://doi.org/10.1016/j.supflu.2020.104847

Pi WM, Wu LY, Lu JH, et al., 2023. A metal ions-mediated natural small molecules carrier-free injectable hydrogel achieving laser-mediated photo-fenton-like anticancer therapy by

synergy apoptosis/cuproptosis/anti-inflammation. *Bioact Mater*, 29:98-115. https://doi.org/10.1016/j.bioactmat.2023.06.018

Platzman I, Brener R, Haick H, et al., 2008. Oxidation of polycrystalline copper thin films at ambient conditions. *J Phys Chem C*, 112(4):1101-1108. https://doi.org/10.1021/jp076981k

Ramírez-García PD, Retamal JS, Shenoy P, et al., 2019. A pH-responsive nanoparticle targets the neurokinin 1 receptor in endosomes to prevent chronic pain. *Nat Nanotechnol*, 14(12):1150-1159. https://doi.org/10.1038/s41565-019-0568-x

Robinson P, Coveñas R, Muñoz M, 2023. Combination therapy of chemotherapy or radiotherapy and the neurokinin-1 receptor antagonist aprepitant: a new antitumor strategy? *Curr Med Chem*, 30(16):1798-1812. https://doi.org/10.2174/0929867329666220811152602

Shadle CR, Murphy MG, Liu Y, et al., 2012. A single-dose bioequivalence and food effect study with aprepitant and fosaprepitant dimeglumine in healthy young adult subjects. *Clin Pharmacol Drug Dev*, 1(3):93-101. https://doi.org/10.1177/2160763X12447304

Shi Y, Wang X, Meng YM, et al., 2021. A novel mechanism of endoplasmic reticulum stress- and c-Myc-degradation-mediated therapeutic benefits of antineurokinin-1 receptor drugs in colorectal cancer. *Adv Sci (Weinh)*, 8(21): e2101936. https://doi.org/10.1002/advs.202101936

Su WQ, Xu P, Petzold R, et al., 2023. Ligand-to-copper charge-transfer-enabled C–H sulfoximination of arenes. *Org Lett*, 25(6):1025-1029. https://doi.org/10.1021/acs.orglett.3c00256

Sun XQ, Gao XH, Wang YY, et al., 2022. Study of the mechanism of nitrogen doping in carbon supports on promoting electrocatalytic oxygen reduction reaction over platinum nanoparticles. *J Fuel Chem Technol*, 50(11):1427-1436. https://doi.org/10.1016/S1872-5813(22)60030-6

Tong F, Hu HL, Xu YY, et al., 2023. Hollow copper sulfide nanoparticles carrying ISRIB for the sensitized photothermal therapy of breast cancer and brain metastases through inhibiting stress granule formation and reprogramming tumor-associated macrophages. *Acta Pharm Sin B*, 13(8):3471-3488. https://doi.org/10.1016/j.apsb.2022.11.003

Tsvetkov P, Coy S, Petrova B, et al., 2022. Copper induces cell death by targeting lipoylated TCA cycle proteins. *Science*, 375(6586):1254-1261. https://doi.org/10.1126/science.abf0529

Upadhyay LSB, Kumar N, 2017. Green synthesis of copper nanoparticle using glucose and polyvinylpyrrolidone (PVP). *Inorg Nano-Metal Chem*, 47(10):1436-1440. https://doi.org/10.1080/24701556.2017.1357576

Wang YT, Zhou W, Jia RR, et al., 2020. Unveiling the activity origin of a copper-based electrocatalyst for selective nitrate reduction to ammonia. *Angew Chem Int Ed*, 59(13): 5350-5354. https://doi.org/10.1002/anie.201915992

Wong KY, Nie ZY, Wong MS, et al., 2024. Metal–drug coordination nanoparticles and hydrogels for enhanced delivery. *Adv Mater*, 36(26):2404053. https://doi.org/10.1002/adma.202404053

Xie JM, Yang YN, Gao YB, et al., 2023. Cuproptosis: mechanisms and links with cancers. *Mol Cancer*, 22:46. https://doi.org/10.1186/s12943-023-01732-y

Yang LF, Yang PP, Lip GYH, et al., 2023. Copper homeostasis and cuproptosis in cardiovascular disease therapeutics. *Trends Pharmacol Sci*, 44(9):573-585. https://doi.org/10.1016/j.tips.2023.07.004

Yang WC, Wang YX, Huang YZ, et al., 2023. 4-Octyl itaconate inhibits aerobic glycolysis by targeting GAPDH to promote cuproptosis in colorectal cancer. *Biomed Pharmacother*, 159:114301. https://doi.org/10.1016/j.biopha.2023.114301

Yarwood RE, Imlach WL, Lieu T, et al., 2017. Endosomal signaling of the receptor for calcitonin gene-related peptide mediates pain transmission. *Proc Natl Acad Sci USA*, 114(46):12309-12314. https://doi.org/10.1073/pnas.1706656114

Yeo S, An J, Park C, et al., 2020. Design and characterization of phosphatidylcholine-based solid dispersions of aprepitant for enhanced solubility and dissolution. *Pharmaceutics*, 12(5):407. https://doi.org/10.3390/pharmaceutics12050407

Yuan DM, Li Q, Zhang Q, et al., 2016. Efficacy and safety of neurokinin-1 receptor antagonists for prevention of chemotherapy-induced nausea and vomiting: systematic review and meta-analysis of randomized controlled trials. *Asian Pac J Cancer Prev*, 17(4):1661-1675. https://doi.org/10.7314/apjcp.2016.17.4.1661

Zhang Y, Zhou Q, Lu L, et al., 2023. Copper induces cognitive impairment in mice via modulation of cuproptosis and CREB signaling. *Nutrients*, 15(4):972. https://doi.org/10.3390/nu15040972

Zheng HQ, Gao CB, Peng BW, et al., 2011. pH-responsive drug delivery system based on coordination bonding in a mesostructured surfactant/silica hybrid. *J Phys Chem C*, 115(15):7230-7237. https://doi.org/10.1021/jp110808f

Zheng HQ, Xing L, Cao YY, et al., 2013. Coordination bonding based pH-responsive drug delivery systems. *Coordin Chem Rev*, 257(11):1933-1944. https://doi.org/10.1016/j.ccr.2013.03.007

Zhou ZQ, Gong F, Zhang P, et al., 2022. Natural product curcumin-based coordination nanoparticles for treating osteoarthritis via targeting Nrf2 and blocking NLRP3 inflammasome. *Nano Res*, 15(4):3338-3345. https://doi.org/10.1007/s12274-021-3864-3

Zhu Y, Niu XG, Ding CY, et al., 2024a. Carrier-free self-assembly nano-sonosensitizers for sonodynamic-amplified cuproptosis-ferroptosis in glioblastoma therapy. *Adv Sci (Weinh)*, 11(23):2402516. https://doi.org/10.1002/advs.202402516

Zhu Y, Niu XG, Wu TT, et al., 2024b. Metal-phenolic nanocatalyst rewires metabolic vulnerability for catalytically amplified ferroptosis. *Chem Eng J*, 485:150126. https://doi.org/10.1016/j.cej.2024.150126

Supplementary information

Materials and methods; Figs. S1 and S2